A Finite Difference Method for Solving Unsteady Viscous Flow Problems

C. P. Li*
NASA Lyndon B. Johnson Space Center, Houston, Texas

A method has been developed to solve the unsteady, compressible Navier-Stokes equations with the property of consistency and the ability of minimizing the equation stiffness. It relies on innovative extensions of the state-of-the-art finite difference techniques and is composed of 1) the upwind scheme for split flux and the central scheme for conventional flux terms in the inviscid and viscous regions, respectively; 2) the characteristic treatment of both inviscid and viscous boundaries; 3) an ADI procedure compatible with interior and boundary points; 4) a scalar matrix solver including viscous terms. The performance of this method is assessed with three sample problems: a shock reflected from the wall, the shock-induced boundary-layer separation, and a transient internal nozzle flow. The results from the present method, an existing hybrid block method, and a well-known two-step explicit method are compared and discussed. It is concluded that this method has an optimal tradeoff between the solution accuracy and computational economy, and other desirable properties for analyzing transient viscous flow problems.

Nomenclature

A	= duct area
$\bar{A},\bar{B},\bar{C},\bar{D}$	= Jacobian matrices
a	= positive integer defined following Eq. (3)
C_F	= friction coefficient
C_v	= specific heat at constant volume
c	= sonic speed
CFL	= Courant-Friedricks-Lewy parameter used to limit magnitude of Δt
E	= explicit method
e	= internal energy
F,G	= convective fluxes
H	= height
I	= implicit method
J	= Jacobian of the transformation
L	= length
ℓ	= number of steps, or split components
M	= freestream Mach number
P	= Jacobian matrix
Pr	= Prandtl number
p	= pressure
Re	= Reynolds number
S,T	= transformation matrices
T	= temperature
t	= time
U	= conservative variable
u,v	= velocity component along x and y, respectively
$\bar{u},\bar{v}$	= velocity component along ξ and η, respectively
V	= primitive variable
W	= characteristic variable
x,y	= cylindrical coordinates
$\alpha_1,\alpha_2,\alpha_3$	= coefficients defined following Eq. (13)
γ	= ratio of specific heat
$\Delta U_{i,j}^{\ell+1},\Delta V_{i,j}^{\ell+1}$	= incremental vectors
δ_ξ,δ_η	= difference operators
ϵ	= total internal energy
θ	= shock angle
κ	= either ξ or η, or conductivity
Λ_ξ,Λ_η	= matrices defined in Eq. (4)
$\lambda_{\xi\ell},\lambda_{\eta\ell}$	= eigenvalues of flux F and G
μ	= viscosity
ξ,η	= generalized computational coordinates
ρ	= density

Superscripts

T	= transpose
$(\ )^*$	= temporary value
$(\bar{\ })$	= computational space

Subscripts

i,j	= grid-point location
∞	= freestream

Introduction

IN many important and interesting compressible flow problems, the unsteady, viscous, and heat-conduction features play a dominant role in the flow behavior. The resulting phenomena have been frequently claimed to be responsible for the unexpected poor performance of aircraft and propulsion devices and, consequently, subjected to extensive experimental and numerical studies. The numerical investigation often requires the solution of the time-dependent Navier-Stokes equations, for which the present methods are not quite powerful enough for engineering applications. One recent attempt to analyze the internal flow of a rocket engine during the startup process has addressed the difficulties encountered.[1] It has found that numerical accuracy and stability bound should be varied according to local flow characteristics and adjusted to suit the flowfield evolution. Since existing methods are incapable of satisfying both requirements simultaneously, a method representing an optimal tradeoff between computation efficiency and solution accuracy is needed to study the transient behavior of viscous flows.

The approach taken to devise such a method is simply to retain some of the useful features in the state-of-the-art techniques for solving fluid-dynamic equations, and introduce innovative ideas that may enhance the existing ones. This is considered a worthwhile effort because in the numerical solution of partial differential equations, the full potential of the finite

Presented as Paper 83-0560 at the AIAA 21st Aerospace Sciences Meeting, Reno, Nev., Jan. 10-13, 1983; received April 7, 1983; revision received June 19, 1984. This paper is declared a work of the U.S. Government and therefore is in the public domain.

*Research Engineer, Thermal Technology Branch. Member AIAA.

difference method has not been realized and the development of numerical approximations is far from complete. An advancement of fundamental value is known to be difficult because the progress has long been hampered by a lack of nonlinear stability and accuracy analyses for boundary-value problems. Furthermore, on the level of practice, the finite difference method is noted to be inefficient for calculating small-scale phenomena and is primitive in the handling of shocks and other discontinuities. Despite the inherent limitations, substantial improvement has been made recently to reduce the equation stiffness[2-4] and to refine the shock-capturing capability.[5-8] By further modifying those techniques, a finite difference method is proposed for analyzing transient, viscous/inviscid external and internal flow problems. This method relies on the following ideas: 1) the upwind scheme for inviscid split flux and the central scheme for viscous flux terms; 2) a characteristic treatment of inviscid and viscous boundaries based on the split formulation; 3) a noniterative ADI procedure with consistent explicit and implicit operators; and 4) a scalar tri- or pentadiagonal solver including viscous contributions. The present formulation is different from that used in Refs. 3-8, the treatment of boundaries is an extension of that discussed in Refs. 9 and 10 to viscous flows, and the implicit solution has an improved algorithm compared with that developed in Refs. 4 and 8. A short description of other important details follows.

The governing equations are cast in generalized coordinates fitted to the solid surface or the interface between streams of different speed. Thereby, the delineation of inviscid and viscous zones is readily accomplished. The split convective fluxes are used in the inviscid zone as well as on the computational boundaries wherein the inward-running flux components are discarded and dependent variables are prescribed. Both convective and diffusion fluxes in the viscous zone are approximated by central differencing and appended with two fourth-order negative derivatives. The difference approximations are made of the explicit operators on the right-hand side of the equations with equivalent implicit operators on the left-hand side. One type of implicit operator is used for a coordinate line, whereas the operators are required to be consistent with the explicit counterparts for most of the interior and boundary points. Thus, the matrix coefficient of the resulting algebraic equations has a pentadiagonal band structure after the equations are decoupled. In addition, conventional implicit central operators requiring the use of a block solver for a coupled set of algebraic equations and an explicit solution based on the MacCormack scheme are included for comparative studies.

In the following sections, the governing equations for inviscid and viscous flows, difference approximations for interior and boundary points, the noniterative ADI procedure, and the algorithm for solving scalar equations are presented. This method and two alternate methods have been tested by inviscid and viscous flow problems with increasing level of difficulty to determine the capability and limitations of the present method. Comparison among the three methods and with analytical and experimental data is also discussed.

Governing Equations in Computational Domain

A boundary-fitted coordinate system is adapted for dual purposes of implementing boundary conditions and defining inviscid and viscous regions. The coordinates are obtained via a transformation function from the physical to the computational spaces by solving the Poisson equation in ξ and η for x and y. The computer code[11] GRAPE is used to generate two-dimensional grids for configurations such as a nozzle configuration, but, for simple geometries, the grids are obtained from algebraic relations. The metric coefficients x_ξ, x_η, y_ξ, y_η are first calculated using finite difference formulas, then substituted to the following relation to obtain ξ_x, ξ_y, η_x, η_y.

$$\begin{bmatrix} \frac{\partial}{\partial x} \\ \frac{\partial}{\partial y} \end{bmatrix} = \begin{bmatrix} \xi_x & \eta_x \\ \xi_y & \eta_y \end{bmatrix} \begin{bmatrix} \frac{\partial}{\partial \xi} \\ \frac{\partial}{\partial \eta} \end{bmatrix} = \frac{1}{J} \begin{bmatrix} y_\eta & -y_\xi \\ -x_\eta & x_\xi \end{bmatrix} \begin{bmatrix} \frac{\partial}{\partial \xi} \\ \frac{\partial}{\partial \eta} \end{bmatrix} \tag{1}$$

where $J = x_\xi y_\eta - x_\eta y_\xi$ is the Jacobian of the transformation. The transformation matrices are used in formulating the governing equations and applying the boundary conditions, as will be seen later.

Two forms of the conservative-law equations cast in generalized computational coordinates (ξ,η) are given next. They are derived with the aid of Eq. (1) from the equations originally written on the cylindrical coordinates (x,y). Hence, the vectors still have components defined in (x,y). For the computation domain where viscous effects cannot be ignored, the following equations in vector notation are used.

$$U_t + (\bar{F} + \bar{F}_v)_\xi + (\bar{G} + \bar{G}_v)_\eta + \bar{S} = 0 \tag{2}$$

where

$$U = J \begin{bmatrix} \rho \\ \rho u \\ \rho v \\ \rho \epsilon \end{bmatrix}, \quad \bar{F} = J \begin{bmatrix} \rho \bar{u} \\ \rho u \bar{u} + \xi_x p \\ \rho v \bar{u} + \xi_y p \\ (\rho \epsilon + p) \bar{u} \end{bmatrix}, \quad \bar{G} = J \begin{bmatrix} \rho \bar{v} \\ \rho u \bar{v} + \eta_x p \\ \rho v \bar{v} + \eta_y p \\ (\rho \epsilon + p) \bar{v} \end{bmatrix}$$

$$\bar{S} = \frac{J}{y} \begin{bmatrix} \rho v \\ \rho v u + \Pi_{xy} \\ \rho v^2 + \Pi_{yy} - \Pi_{zz} \\ (\rho \epsilon + p) v + \phi_y \end{bmatrix} \quad \bar{F}_v = J \begin{bmatrix} 0 \\ \xi_x \Pi_{xx} + \xi_y \Pi_{xy} \\ \xi_x \Pi_{xy} + \xi_y \Pi_{yy} \\ \xi_x \phi_x + \xi_y \phi_y \end{bmatrix}$$

$$\bar{G}_v = J \begin{bmatrix} 0 \\ \eta_x \Pi_{xx} + \eta_y \Pi_{xy} \\ \eta_x \Pi_{xy} + \eta_y \Pi_{yy} \\ \eta_x \phi_x + \eta_y \phi_y \end{bmatrix}$$

When the viscous effects are negligible in other portions of the computational domain, then the Euler equation in the flux-split form is used.

$$U_t + \bar{F}_\xi + \bar{G}_\eta + \bar{S} = 0 \tag{3}$$

where

$$\bar{F} = J\rho \sum_{\ell=-1}^{1} \gamma_\ell \lambda_{\xi\ell} \begin{bmatrix} 1 \\ u + \ell c \xi_x \\ v + \ell c \xi_y \\ q + \ell \bar{u} c / \xi + |\ell| \gamma e \end{bmatrix}$$

$$\bar{G} = J\rho \sum_{\ell=-1}^{1} \gamma_\ell \lambda_{\eta\ell} \begin{bmatrix} 1 \\ u + \ell c \eta_x \\ v + \ell c \eta_y \\ q + \ell \bar{v} c / \bar{\eta} + |\ell| \gamma e \end{bmatrix}$$

where

$$\gamma_\ell = (1 - |\ell|)(\gamma - 1)/\gamma + |\ell|/(2\gamma)$$

$$\lambda_{\xi\ell}=\bar{u}+\ell c\bar{\xi},\quad \lambda_{\eta\ell}=\bar{v}+\ell c\bar{\eta}$$

$$\bar{u}=\xi_x u+a\xi_y v,\quad \bar{v}=\eta_x u+a\eta_y v$$

$$\bar{\xi}_x=\xi_x/\bar{\xi},\quad \bar{\xi}_y=\xi_y/\bar{\xi},\quad \bar{\xi}=(\xi_x^2+\xi_y^2)^{1/2}$$

$$\bar{\eta}_x=\eta_x/\bar{\eta},\quad \bar{\eta}_y=\eta_y/\bar{\eta},\quad \bar{\eta}=(\eta_x^2+\eta_y^2)^{1/2}$$

$$a=1 \text{ if } y\neq 0,\quad a=2 \text{ if } y=0$$

Conventional notation is used here for flow variables; viz., the density ρ, the pressure p, and the velocity components u and v in the cylindrical system; the total internal energy $\epsilon=e+0.5q$, and $q=u^2+v^2$, and the internal energy $e=C_vT$, which relates to p and ρ by the equation of state. The sonic speed is $c=(\gamma p/\rho)^{1/2}$; γ is the ratio of specific heat. The stress and heat-conducting components are also given first in the physical coordinates. Then, they are computed in their transformed form via Eq. (1). The lengthy expressions of these components will not be given here, except to note that Sutherland's formula for viscosity coefficient and a Prandtl number ($Pr=0.71$) are used for laminar flow computations.

The eigenvalues of fluxes $\bar{F}$ and $\bar{G}$ defined in Eq. (3) are $\lambda_{\xi\ell}$ and $\lambda_{\eta\ell}$, respectively. They are conventionally regarded as components in the eigenmatrices

$$\Lambda_\xi=\text{diag}\,(\bar{u}-c\bar{\xi},\ \bar{u},\ \bar{u},\ \bar{u}+c\bar{\xi})$$

$$\Lambda_\eta=\text{diag}\,(\bar{v}-c\bar{\eta},\ \bar{v},\ \bar{v},\ \bar{v}+c\bar{\eta}) \tag{4}$$

On the axis of symmetry, $y=0$, it is required that $v=0$ and the eigenmatrices have three instead of four components.

Equations (2) and (3) can be easily modified to consider one-dimensional problems. For a simple, inviscid flow in the Laval duct, Eq. (3) is reduced to

$$U_t+\bar{F}_\xi+S=0 \tag{5}$$

where

$$U=\begin{bmatrix}\rho\\ \rho u\\ \rho\epsilon\end{bmatrix},\quad \bar{F}=\rho\sum_{-1}^{1}\gamma_\ell\lambda_{\xi\ell}\begin{bmatrix}1\\ u+\ell c\\ q+\ell\bar{u}c+|\ell|\gamma e\end{bmatrix}$$

$$S=\frac{A_\xi}{A}\begin{bmatrix}\rho u\\ \rho u^2\\ \rho u\epsilon+pu\end{bmatrix}$$

with $\lambda_{\xi\ell}=\bar{u}+\ell c$ and A being the duct area. Here, the Jacobian and the metrics are equal to unity and the flux term in the η coordinate is dropped out. If it is considered that U has a third component v but $v=0$, then Eq. (5) becomes a special case of Eq. (3). The solution algorithm developed for two-dimensional problems is equally applicable to one-dimensional problems.

Boundary and Initial Conditions

The dependent variables on the boundaries are determined in accordance with the flow speed and the nature of the boundary, or known as the method of characteristics. For convenience of discussion, the types of boundaries are referred to as solid surface, inflow and outflow surfaces, and plane of symmetry. If Eq. (3) has four outward-running components on the flow boundaries, no boundary condition is needed. Otherwise, the number of inward-running components being discarded in the calculation is complemented by an equal number of flow variables specified. More specifically, a subsonic outward flow has $\lambda_4>0$, and the pressure must be given; a subsonic inward flow has $\lambda_{2,3,4}>0$, and both pressure and velocity components must be known. Furthermore, if the inward flow is supersonic, i.e., $\lambda_{1,2,3,4}>0$, then every variable must be specified a priori. The rules are summarized in Table 1.

The consideration of characteristics is also useful in the calculation of variables on a solid surface. There, the inviscid tangency condition $\bar{v}=0$ implies that the conditions $\lambda_{2,3}=0$ and $\lambda_1<0$ permit a readjustment of velocity components in the physical space by

$$\begin{bmatrix}u\\ v\end{bmatrix}=J\begin{bmatrix}\eta_y & -\xi_y\\ -\eta_x & \xi_x\end{bmatrix}\begin{bmatrix}\bar{u}\\ \bar{v}\end{bmatrix}$$

after substituting $\bar{v}=0$.

The viscous no-slip condition is usually applied in conjunction with an adiabatic or a cooled-wall condition in temperature. The remaining variable, ρ, can be obtained by assuming zero pressure gradient at the wall. On the inflow and outflow surfaces, viscous flow may exist in the boundary layer; therefore, it is assumed in this study that the conditions imposed by the method of characteristics are still valid.

Initial conditions are specified such that they simulate the realistic beginning of the unsteady flow. The flowfield is uniform until at $t=0$, when the shock generated by a wedge at a distance above a plate begins to form and reflect from the plate, or the flowfield is quiescent until a shock propagates out from the throat of the nozzle.

Explicit Difference Operators and Stability Conditions

Let RHS designate the difference equations approximating Eqs. (2) and (3) on a typical uniform grid (Fig. 1) wherein $\xi_i=(i-1)\Delta\xi$ and $\eta_j=(j-2)\Delta\eta$.

$$\text{RHS } 1=-[\delta_\xi(\bar{F}+\bar{F}_v)+\delta_\eta(\bar{G}+\bar{G}_v)+\bar{S}^\ell_{i,j}]\Delta t$$

$$\text{RHS } 2=-\left[\sum_{\ell=-1}^{1}\delta_\xi(\bar{F}_\ell)+\sum_{\ell=-1}^{1}\delta_\eta(\bar{G}_\ell)+\bar{S}^\ell_{i,j}\right]\Delta t \tag{6}$$

The difference operator δ_ξ has a variety of expressions depending on what flux it governs. The inviscid operators are given by either Eq. (7) or Eq. (8).

$$\delta_\xi\bar{F}=[1/(2\Delta\xi)]\,[\bar{F}_{i+1,j}-\bar{F}_{i-1,j}] \tag{7}$$

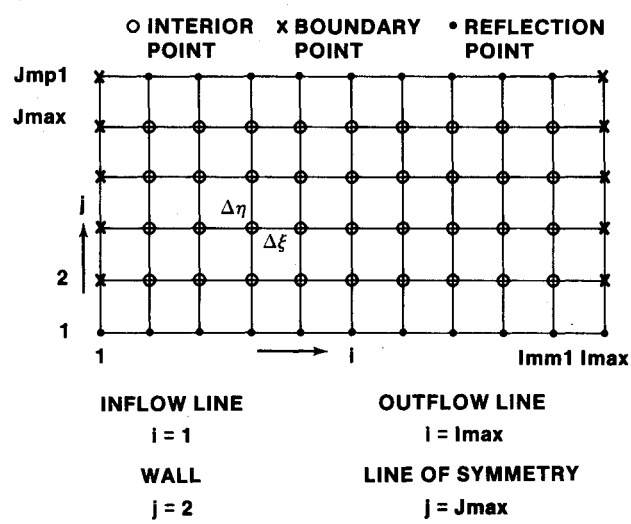

Fig. 1 Computational grid network.

$$\delta_\xi(\bar{F}_\ell) = (IS/\Delta\xi)[(\bar{F}_\ell)_{i,j} - (\bar{F}_\ell)_{i-IS,j}] + 0(\Delta\xi^2)$$
$$= (IS/2\Delta\xi)[3(\bar{F}_\ell)_{i,j} - 4(\bar{F}_\ell)_{i-IS,j} + (\bar{F}_\ell)_{i-2*IS,j}] + 0(\Delta\xi^3) \quad (8)$$

where $IS = \text{sgn}(1,\lambda_\ell)$. The viscous fluxes are approximated by central differencing formulas, such as

$$\delta_\xi \bar{F}_v = (1/\Delta\xi)[(\bar{F}_v)_{i+1/2,j} - (\bar{F}_v)_{i-1/2,j}] \quad (9)$$

More detailed expressions for terms in $\bar{F}_v$ are defined by the following.

$$\delta_\xi(\mu\delta_\xi u) = \frac{1}{\Delta\xi}\left[\frac{\mu_{i+1,j}+\mu_{i,j}}{2}\,\frac{u_{i+1,j}-u_{i,j}}{\Delta\xi} - \frac{\mu_{i,j}+\mu_{i-1,j}}{2}\,\frac{u_{i,j}-u_{i-1,j}}{\Delta\xi}\right]$$

$$\delta_\xi(\mu\delta_\eta u) = \frac{1}{\Delta\xi}\left[\frac{\mu_{i+1,j}+\mu_{i,j}}{2}\,\frac{u_{i+1,j+1}-u_{i+1,j-1}+u_{i,j+1}-u_{i,j-1}}{4\Delta\eta} - \frac{u_{i,j}+\mu_{i-1,j}}{2}\,\frac{u_{i,j+1}-u_{i,j-1}+u_{i-1,j+1}-u_{i-1,j-1}}{4\Delta\eta}\right] \quad (10)$$

They are the conventional three-point quotient for $\delta_{\xi\xi}$ and $\delta_{\eta\eta}$ and the four-point quotient for $\delta_{\xi\eta}$.

Equation (7) is replaced by a one-sided difference formula for points on the boundary.

$$\delta_\xi \bar{F} = \frac{1}{\xi_{i\pm1} - \xi_i}[\bar{F}_{i\pm1,j} - \bar{F}_{i,j}], \quad 1 \le i \pm 1 \le I\max$$

Likewise, Eq. (9) becomes

$$\delta_\xi \bar{F}_v = \frac{2}{\xi_i - \xi_{i\pm1/2}}[(\bar{F}_v)_{i\pm1/2,j} - (\bar{F}_v)_{i\pm3/2,j}], \quad 1 \le i \pm 2 \le I\max$$

The operator δ_η is defined similarly to Eqs. (7-9). However, one-sided difference quotients are not used because a grid line is placed outside the boundary to help define boundary conditions. The viscous operators given by RHS 1 in Eq. (6) are used with fourth-order damping terms in ξ and η. These terms are defined for interior points as: $-(\xi_d(\Delta\xi)^4\delta_{\xi\xi\xi\xi}U)/8$ and $-(\eta_d(\Delta\eta)^4\delta_{\eta\eta\eta\eta}U)/8$.

In explicit calculations, Eq. (6) represents the incremental vector, $\Delta U_{i,j}^{\ell+1}$, defined by

$$\Delta U_{i,j}^{\ell+1} = U_{i,j}^{\ell+1} - U_{i,j}^{\ell} = \text{RHS}$$

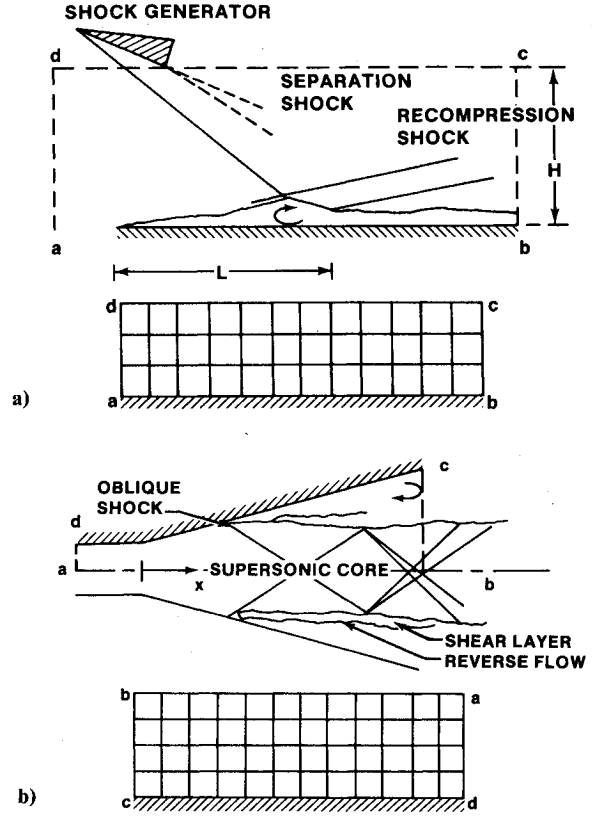

Fig. 2 Sample problems in physical and computational spaces. a) Shock reflection and boundary-layer separation [$\xi = \xi(x)$, $\eta = \eta(y)$]. b) Transient viscous nozzle flow [$\xi = \xi(x,y)$, $\eta = \eta(x,y)$].

Table 1 Boundary conditions needed on inflow and outflow boundaries

Speed[a]	Signal propagation[b]	Description	Specified boundary conditions
$\tilde{u} > \tilde{c}$	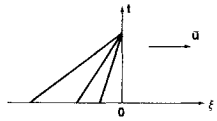	Supersonic inflow $\lambda_{1,2,3,4} > 0$	ρ, u, v, e
$0 < \tilde{u} < \tilde{c}$	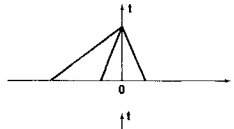	Subsonic inflow $\lambda_{2,3,4} > 0$, $\lambda_1 < 0$	p, u, v
$-\tilde{c} < \tilde{u} < 0$	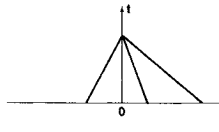	Subsonic outflow $\lambda_4 > 0$, $\lambda_{1,2,3} < 0$	p
$\tilde{u} < -\tilde{c}$	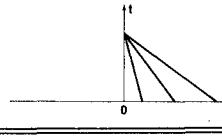	Supersonic outflow $\lambda_{1,2,3,4} < 0$	None

[a] $\tilde{c} = c(\xi_x^2 + \xi_y^2)^{1/2}$, $\tilde{u} = \xi_x u + \xi_y v$. [b] Computational domain defined by $\xi \ge 0$.

for time $t=\ell\Delta t$. The time increment Δt is determined from a nonconventional relationship that satisfies the stability conditions for a linear difference equation. A parameter CFL is introduced to limit the magnitude of Δt for a stable solution

$$\Delta t = \text{CFL} \times \min\left[\frac{1}{|\bar{\Lambda}_\xi|_\ell}, \frac{1}{|\bar{\Lambda}_\eta|_\ell}\right] i,j$$

Note that the first-order scheme requires CFL ≤ 0.5 and the second-order scheme requires CFL ≤ 0.25. However, a higher bound CFL ≤ 1 can be used by a two-step noncentered scheme. Thus, in practical applications, the latter scheme is preferable to those in Eq. (8), unless an implicit algorithm is developed to extend the stability bound.

An ADI Scalar Method

The second stage of the solution procedure is used to remove or filter out the error components in $\Delta U_{i,j}^{\ell+1}$ when the explicit calculations at some grid points have violated the domain of influence of the known $U_{i,j}^{\ell}$. It is accomplished by solving for $\Delta U_{i,j}^{\ell+1}$ simultaneously for all i and j; thereby, the domain of influence is literally enlarged. Using $\Delta U_{i,j}^{\ell+1}$ as the unknown vector, the implicit equation is cast in the following matrix-operator form

$$(\delta_t + \bar{A}\delta_\xi + \bar{B}\delta_\eta - \bar{C}\delta_{\xi\xi} - \bar{D}\delta_{\eta\eta})\Delta V_{i,j}^{\ell+1} = P^{-1}\Delta U_{i,j}^{\ell+1} = \Delta V_{i,j}^{\ell+1} \quad (11)$$

$\bar{A}$, $\bar{B}$, $\bar{C}$, $\bar{D}$, and P^{-1} are the Jacobian matrices derived from the derivative of $\bar{F}$, $\bar{G}$, $\bar{F}_v$, $\bar{G}_v$, and U with respect to V, respectively. Their expressions are listed as follows.

$$P^{-1} = \frac{1}{J\rho}\begin{bmatrix} \rho & 0 & 0 & 0 \\ -u & 1 & 0 & 0 \\ -v & 0 & 1 & 0 \\ -e+q & -u & -v & 1 \end{bmatrix}$$

$$\bar{A} = \begin{bmatrix} \bar{u} & \xi_x\rho & \xi_y\rho & 0 \\ \xi_x h & \bar{u} & 0 & \xi_x g \\ \xi_y h & 0 & \bar{u} & \xi_y g \\ 0 & \xi_x f & \xi_y f & \bar{u} \end{bmatrix}, \quad \bar{B} = \begin{bmatrix} \bar{v} & \eta_x\rho & \eta_y\rho & 0 \\ \eta_x h & \bar{v} & 0 & \eta_x g \\ \eta_y h & 0 & \bar{v} & \eta_y g \\ 0 & \eta_x f & \eta_y f & \bar{v} \end{bmatrix}$$

$$\bar{C} = \frac{1}{\rho}\begin{bmatrix} 0 & 0 & 0 & 0 \\ 0 & \mu(4\xi_x^2/3+\xi_y^2) & 0 & 0 \\ 0 & 0 & \mu(\xi_x^2+4\xi_y^2/3) & 0 \\ 0 & 0 & 0 & \kappa(\xi_x^2+\xi_y^2) \end{bmatrix}$$

$$\bar{D} = \frac{1}{\rho}\begin{bmatrix} 0 & 0 & 0 & 0 \\ 0 & \mu(4\eta_x^2/3+\eta_y^2) & 0 & 0 \\ 0 & 0 & \mu(\eta_x^2+4\eta_y^2/3) & 0 \\ 0 & 0 & 0 & \kappa(\eta_x^2+\eta_y^2) \end{bmatrix}$$

where $f=p/\rho$, $g=\gamma-1$, and $h=ge/\rho$. The unknown vector is $\Delta V_{i,j}^{\ell+1}$, where $V=(\rho,u,v,e)^T$. The use of the incremental vector is preferable to the use of the vector itself, because the small value of ΔV compared to V makes more precise arithmetics.

Since it is still time consuming to solve the coupled algebraic systems of equations as given by Eq. (11) using the approximate factorization technique,[3] especially when the number of variables is large, the property of a real matrix coefficient is exploited to allow the following transformations: $T^{-1}\bar{A}T=\bar{\Lambda}_\xi$ and $S^{-1}\bar{B}S=\bar{\Lambda}_\eta$. The inclusion of viscous terms is made possible from heuristic reasonings that

$$\bar{C} \cong \frac{\mu}{\rho}(\xi_x^2+\xi_y^2)I \equiv \nu_\xi I, \quad \bar{D} \cong \frac{\mu}{\rho}(\eta_x^2+\eta_y^2)I \equiv \nu_\eta I$$

Thus, the left-hand side of the equation is factored into

$$\text{LHS} = (I + \Delta t T\bar{\Lambda}_\xi T^{-1}\delta_\xi + \Delta t S\bar{\Lambda}_\eta S^{-1}\delta_\eta)\Delta V_{i,j}^{\ell+1}$$

$$= T(I+\Delta t\bar{\Lambda}_\xi\delta_\xi)T^{-1}S(I+\Delta t\bar{\Lambda}_\eta\delta_\eta)S^{-1}\Delta V_{i,j}^{\ell+1}$$

where δ_t is replaced by the Euler differencing formula and $\bar{\Lambda}_\xi=\bar{\Lambda}_\xi-\bar{C}\delta_\xi$ and $\bar{\Lambda}_\eta=\bar{\Lambda}_\eta-\bar{D}\delta_\eta$. The second step is the result after exercising the factorization of operators equivalent to the ADI procedure.[4]

The solution procedure for implicit calculation is implemented in four steps.

$$\begin{aligned} &1)\ \Delta V_{i,j}^{*} = P_{i,j}^{-1}(\text{RHS}) \\ &2)\ (I+\Delta t\delta_\xi\bar{\Lambda}_\xi)\Delta W_{i,j}^{*} = T^{-1}\Delta V_{i,j}^{*} \\ &3)\ (I+\Delta t\delta_\eta\bar{\Lambda}_\eta)\Delta W_{i,j} = S^{-1}T\Delta W_{i,j}^{*} \\ &4)\ \Delta V_{i,j}^{\ell+1} = S\Delta W_{i,j} \end{aligned} \quad (12)$$

The first and fourth equations involve simple multiplication between a matrix and a vector. For flow of single-component gas, $\Delta V_{i,j}^{*}$ can be obtained directly from $\Delta U_{i,j}$, and the results are more accurate than that from the first equation.

The transformation matrices S and T are given in the following: let $T=T_\xi$ and $S=T_\eta$; then,

$$T_\kappa = \frac{1}{\sqrt{2}}\begin{bmatrix} -1/\rho & -1/\rho & p/\rho c & p/\rho c \\ 1/e & 1/e & \rho/c & \rho/c \\ -\bar{\kappa}_y & \bar{\kappa}_y & \bar{\kappa}_x & -\bar{\kappa}_x \\ \bar{\kappa}_x & -\bar{\kappa}_x & \bar{\kappa}_y & -\bar{\kappa}_y \end{bmatrix}$$

$$T_\kappa^{-1} = \frac{1}{\sqrt{2}}\begin{bmatrix} -\rho/\gamma & p/\gamma\rho & -\bar{\kappa}_y & \bar{\kappa}_x \\ -\rho/\gamma & p/\gamma\rho & \bar{\kappa}_y & -\bar{\kappa}_x \\ c/\gamma e & c/\gamma\rho & \bar{\kappa}_x & \bar{\kappa}_y \\ c/\gamma e & c/\gamma\rho & -\bar{\kappa}_x & -\bar{\kappa}_y \end{bmatrix}$$

$$T_\kappa^{-1}T_\ell = \frac{1}{2}\begin{bmatrix} 1+m_1 & 1-m_1 & -m_2 & m_2 \\ 1-m_1 & 1+m_1 & m_2 & -m_2 \\ m_2 & -m_2 & 1+m_1 & 1-m_1 \\ -m_2 & m_2 & 1-m_1 & 1+m_1 \end{bmatrix}$$

where $m_1=\bar{\kappa}_x\bar{\ell}_x+\bar{\kappa}_y\bar{\ell}_y$, $m_2=-\bar{\kappa}_x\bar{\ell}_y+\bar{\kappa}_y\bar{\ell}_x$, and $\kappa=\xi$ or η.

Decoupled Simultaneous Equations

The second and third equations in Eq. (12) represent, respectively, the sweeps in i-index and j-index grid points. There are $J\max+(J\max-1)$ sweeps, and the incremental vec-

tor is solved twice. Each sweep involves the solution of $\Delta V_{i,j}$ from a system of algebraic equations. The matrix coefficient of the system has a pentadiagonal band structure, because the upwind scheme uses two points on either side of the diagonal. The ith row of the matrix equation is

$$a_i x_{i-2} + b_i x_{i-1} + c_i x_i + d_i x_{i+1} + e_i x_{i+2} = f_i \qquad (13)$$

where

$$x_i = \Delta W^*_{i,j},\ f_i = \text{RHS of Eq. (12)}$$

$$a_i = \alpha_3(\beta + 0.5)\lambda_{i-2},\quad b_i = \alpha_2(\beta + 0.5)\lambda_{i-1} - \nu_{i-1}$$

$$c_i = 1 + 2\alpha_1\beta\lambda_i + 2\nu_i$$

$$d_i = \alpha_2(\beta - 0.5)\lambda_{i+1} - \nu_{i+1},\quad e_i = \alpha_3(\beta - 0.5)\lambda_{i+2}$$

and

$$\alpha_1 = 1.5,\ \alpha_2 = -2,\ \alpha_3 = 0.5,\ \beta = \text{sgn}(0.5, \lambda_i)$$

$$\lambda_i = \lambda_{\xi i}\Delta t,\ \nu_i = \nu_{\eta i}\Delta t$$

With this procedure, the switching of one-sided differencing is automated according to the direction of λ_i. Note Eq. (13) is used four times in which λ and ν take in turn the components

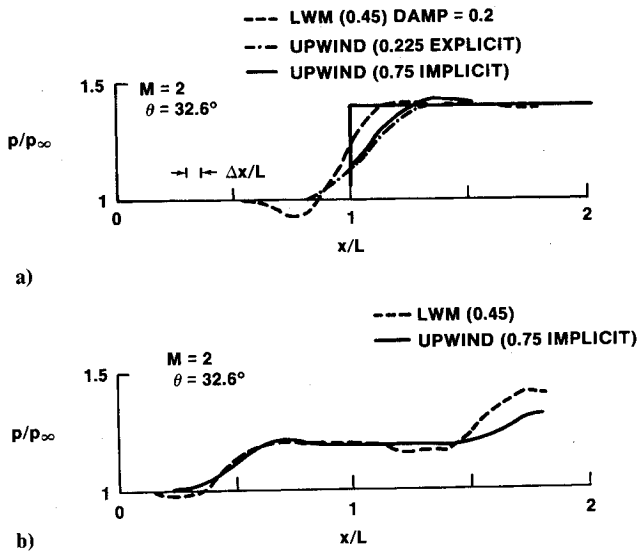

Fig. 3 Comparisons of pressures in the shock reflection problem; a) wall pressure distribution caused by shock reflection; b) pressure distribution on the line $y = H/2$.

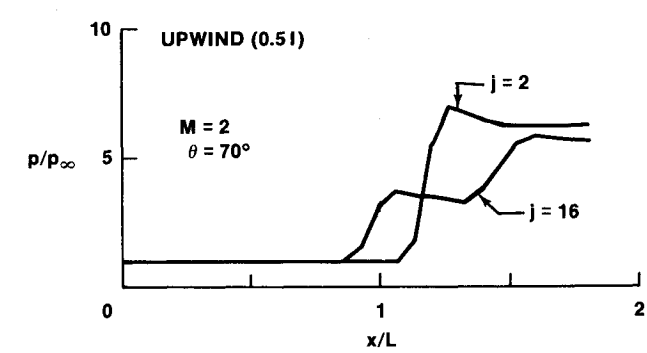

Fig. 4 Pressure distributions on the wall and on $y = H/2$ for a strong shock reflection.

Table 2 Implicit numerical boundary treatment on characteristic variables

Grid line	Physical condition	Treatment
$I=1$	Inflow	$a_1 = b_1 = 0$
$I=I\text{max}$	Outflow	$d_{I\text{max}} = e_{I\text{max}} = 0$
$J=2$	Inviscid wall	$c_2 = c_2 + 2b_2$, $d_2 = d_2 - b_2$, $a_2 = b_2 = 0$
	Viscid wall	$a_2 = b_2 = c_2 = d_2 = e_2 = 0$, $a_3 = b_3 = 0$
$J=J\text{max}$	Symmetry line	$c_{J\text{max}} = c_{J\text{max}} + 2d_{J\text{max}}$, $b_{J\text{max}} = b_{j\text{max}} - d_{J\text{max}}$, $d_{J\text{max}} = e_{J\text{max}} = 0$

of Λ and D from $\ell = 1$ through 4. The same type of equation is used for the jth row of the third matrix equation in Eq. (12), by replacing $\lambda_j = \lambda_{\eta j}\Delta t$, $\nu_j = \nu_{\eta j}\Delta t$, and $x_j = \Delta W_{i,j}$. The solution of Eq. (13) is based on a lower and upper decomposition similar to that used for solving the tridiagonal system of equations.

Sometimes, the conventional central scheme is used instead; the coefficients in Eq. (13) easily can be changed to a form compatible with the central difference. After substituting $\alpha_1 = 1$, $\alpha_2 = -1$, $\alpha_3 = 0$, and $\beta = 0$ into the formulas defining coefficients, Eq. (13) becomes a tridiagonal matrix equation. Furthermore, for the first-order upwind scheme, parameters $\alpha_1 = 1$, $\alpha_2 = 1$, and $\alpha_3 = 0$ will yield a compatible implicit operator.

Numerical Boundary Treatment

The conditions governing $\Delta W^*_{i,j}$ and $\Delta W_{i,j}$ on the boundaries are implemented into Eq. (13) to close the equation system at both ends. Using a typical computational region depicted in Fig. 1, the implicit boundary treatment is summarized in Table 2. Evidently, the fact that the boundary conditions are indirectly related to W has prevented the full account of solid wall to the implicit solution.

To ensure the boundary conditions are satisfied at each integration step (after the implicit step), the following relations in terms of primary variables are enforced.

$$\rho_{i,2} = \rho_{i,3},\ u_{i,2} = v_{i,2} = 0,\ e_{i,2} = e_{i,3}$$

If the variables are not calculated from the inviscid split-flux formulation or from the one-sided viscous formulation, they are obtained from the space extrapolation formula[10]

$$U^{\ell+1}_{I\text{max},j} = 2U^{\ell+1}_{I\text{mm}1,j} - U^{\ell+1}_{I\text{mm}2,j},\qquad U^{\ell+1}_{I\text{max},j} = U^{\ell+1}_{I\text{mm}1,j}$$

where $I\text{mm}1 = I\text{max} - 1$ and $I\text{mm}2 = I\text{max} - 2$. Then, taking into consideration the flow speed and direction on $I = I\text{max}$, additional conditions (Table 1) may be imposed. This procedure has been compared with the one-sided calculation procedure for an outflow boundary with subsonic and viscous flow profile in later sections.

Alternate Methods of Solution

Two existing methods have been adapted to substitute the difference operators discussed previously for the purpose of guiding the development of the present method. The MacCormack 1969 explicit two-step scheme is used to validate the explicit operators,[12] whereas the Beam-Warming method is used to check the implicit operators. Reklis and Thomas[8] have foreseen the problem with too much natural damping in the upwind scheme to adversely affect the accuracy in viscous computation, and proposed a hybrid method of ξ-upwind and

η-central operators. (The present approach, however, does not use explicit upwind operators at all in the viscous region.) Despite various forms of operators in the RHS equation, the LHS equation uses only central operators. The solutions to Eqs. (2) and (3) are obtained from the following two block matrix equations.

$$(I+\delta_\xi \bar{A}-\delta_{\xi\xi}\bar{C})\Delta V^*_{i,j}=P^{-l}_{i,j}\ (\text{RHS})$$

$$(\mathrm{I}+\delta_\eta \bar{B}-\delta_{\eta\eta}\bar{D})\Delta V^{l+1}_{i,j}=\Delta V^*_{i,j} \qquad (14)$$

The equations are solved by a standard tridiagonal block solver, for which a detailed formulation of the matrix coefficient including boundary points is given in Ref. 13.

Discussion of Sample Problems

A computer code has been developed on the UNIVAC 1182 time-sharing system with sufficient flexibility that a variety of one-dimensional and two-dimensional problems can be solved by minimal changes of boundary conditions and metrics. This code also has modular structure to enable the user to switch the calculation algorithm from one to another. The algorithms used herein are referred to the hybrid scalar solver, the hybrid block solver, and the explicit solver. A number of problems have been selected to assess the accuracy and efficiency of the algorithms. They are of varying degree of difficulty in order to expose various aspects of capability and limitations. Two of the sample problems are illustrated in Fig. 2 in both physical and computation spaces. The first problem, not shown here, is a supersonic-subsonic flow in a Laval nozzle. The solutions are obtained from Eq. (5) for Mach 2 upstream flow of the standing shock. The shock width is within 2 to 3 points and free of oscillations. The stability bound is less than that for a similar case reported in Ref. 10, since implicit damping is excluded from Eq. (12).

Shock Reflection on a Wall

A practical problem investigated by Hakkinen et al.[14] in a wind-tunnel environment is solved with both the Euler and the Navier-Stokes equations. The freestream conditions are given by $M=2$, $Re_L=0.296\times10^6$, $L=0.049$ m, and the shock angle $\theta=32.6$ deg. The physical domain (Fig. 2a) is selected to be $x\cong 2.2L$ and $y=H=0.77L$, and the uniform grid is mapped onto a similar uniform computational grid of 32×32. The metric coefficients are calculated to define the computational domain in (32,32). The initial conditions consist of a constant supersonic flow over the plate, and the oblique shock is assigned to be the condition on the top line at $y=H$.

Numerical results of pressure distributions on the wall and on the line $y=0.5H$ are plotted in Fig. 3. The upwind calculations are made with the highest possible CFL numbers allowable for explicit and implicit methods. A quick estimate of the CFL number and the algebraic work required by the methods considered in this study suggests that the present scalar implicit method must use 0.75 or higher for the CFL number in order to be competitive with the explicit two-step upwind method. Comparison made between the central and upwind implicit difference methods reveals that the former is more efficient than the latter method. Another factor influencing the selection of method is the shock-capturing capability in two-dimensional flows. As shown in Fig. 3a, 9 points are needed by the upwind scheme vs 12 points needed by the Lax-Wendroff-MacCormack (LWM) scheme. The undershoot appearing on the pressure profile resembles that in the one-dimensional problem. Not shown in Fig. 3a is the result of the implicit central method, which has reached an erroneous pressure plateau because the second and fourth-order damping needed for eliminating nonlinear instability is too strong to yield accurate solutions. The pressure distributions from the two methods are compared in Fig. 3b. The pressure difference near the outflow boundary is caused by the differences in the

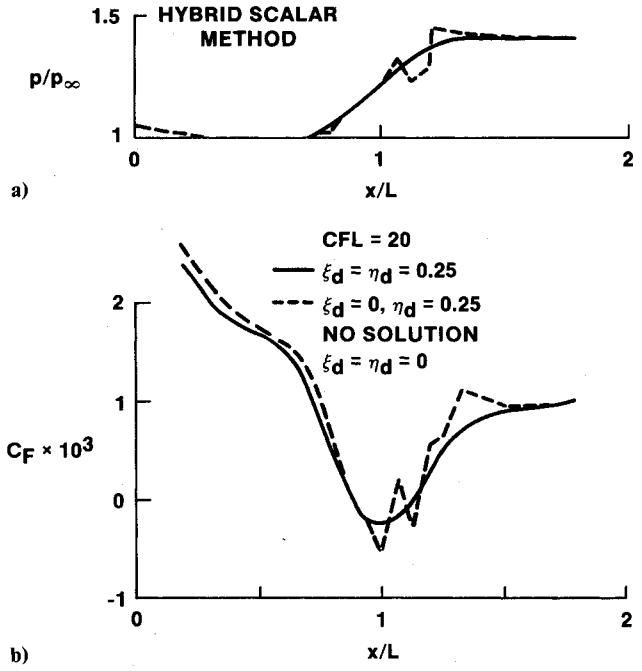

Fig. 5 Investigation of the effect of fourth-order damping on the shock/boundary-layer interaction problem: a) wall pressure distribution; b) friction coefficient on the wall.

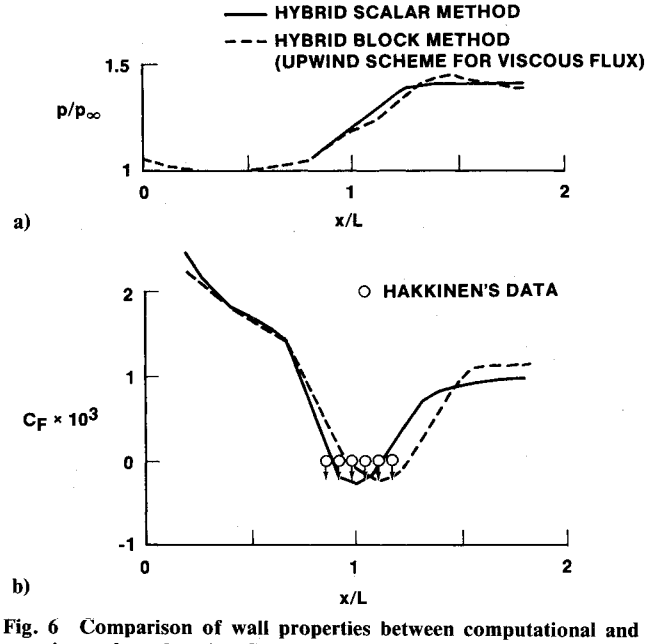

Fig. 6 Comparison of wall properties between computational and experimental results: a) wall pressure distributions; b) friction coefficient distributions on the wall.

equations and in the boundary treatment. The present method predicts the pressure level closer to the theoretical value.

The upwind method is designed to approximate solutions where the characteristic value changes sign across a shock. If the conditions are not right, for instance, the shock strength is weak, some of the desirable properties will disappear. It has been shown in Ref. 15 in one-dimensional experiments and by the two-dimensional case in Fig. 3. To complete the verification of the conjecture, the inviscid calculation is made for $\theta=70$ deg. The pressure distributions obtained (Fig. 4) clearly show sharper profiles of shocks on the wall and on the midline $y=0.5H$. Since the pressure ratios across the shock are much higher than those in the previous case, methods based on cen-

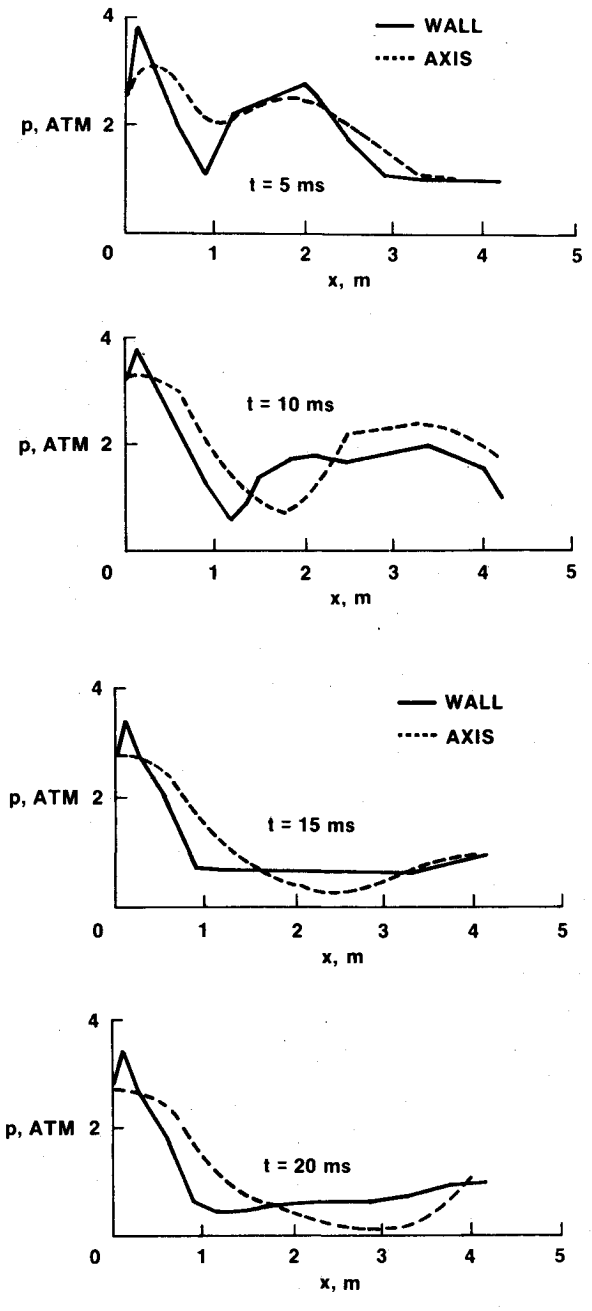

Fig. 7 Nozzle pressure distributions at $t=0.005$, 0.01, 0.015, and 0.02 s obtained from the no-slip model.

tral operators cannot reach steady state after experiencing some forms of instability.

Shock-Induced Boundary-Layer Separation

This problem is similar to the shock reflection problem, except for the inclusion of viscous effect of the wall. The physical grid comprises (32×43) points nonuniformly stretched in y, with $\Delta y_2=0.1\ L/(Re_L)^{1/2}\cong3\times10^{-6}$ m. The computational domain is as before defined on a set of uniform grids (32,43). The hybrid scalar method employs the central scheme between 0 and $0.1H$ in y and the upwind scheme for y greater than $0.1H$. The fourth-order x and y derivatives are found to be very important in damping out the nonlinear instabilities. Presented in Fig. 5 are the pressure and friction coefficients on the wall. Smooth and accurate solutions are obtained with $0.1\leq\xi_d=\eta_d\leq0.25$. Spurious oscillations are found in the solution obtained with $\xi_d=0$, $\eta_d=0.25$. Computations have become unstable if fourth-order damping terms are not used

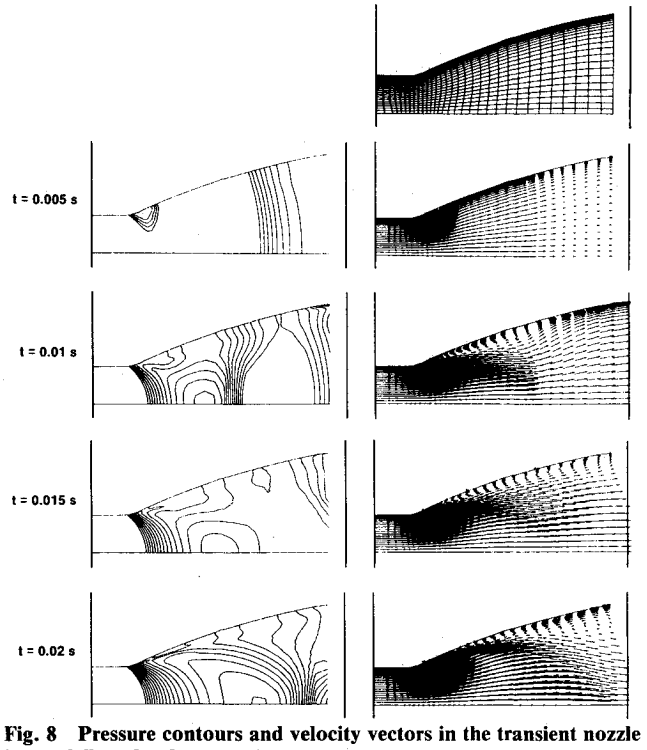

Fig. 8 Pressure contours and velocity vectors in the transient nozzle internal flow development ($\Delta y_2=0.003$ m, $\Delta y_{28}=0.09$ m, 32×28).

at all. The stable solution agrees very well with the experimental data of Hakkinen.[14] The agreement indicates the judicious choice of central and upwind schemes in the present hybrid method. If the hybrid method combines the use of central and upwind schemes in such a way as suggested in Ref. 8, the upwind differencing of x flux in the viscous region will adversely affect the accuracy. There is a rearward shift of friction coefficient predicted by the Reklis and Thomas method shown in Fig. 6b. The shift probably is caused by the use of two different operators in the same region. The computations are made using CFL = 20 and $\ell=600$ steps. The scalar method consumes about two-thirds of computation time used by the block method since the scalar pentadiagonal solver is about ten times faster than the block tridiagonal solver in the two-dimensional case. The majority of computation time is, therefore, spent on the evaluation of transformation matrices, Jacobian matrices, and the explicit incremental vector.

Transient Nozzle Internal Flow

The nozzle configuation illustrated in Fig. 2b has the combustion chamber at the left and the exit to ambient air on the right. This simple model is used to study the unsteady flow behavior during the first few hundred milliseconds, when the rocket motor starts and the flow is moving downstream impulsively.[1] The initial and most of the boundary conditions can be prescribed realistically, whereas for the inflow time-dependent boundary, some assumptions must be made. Other than the chamber total conditions, the inflow boundary may be regarded as the throat having sonic inviscid flow. Fortuitously, neither assumption will prevent the assessment of the code capability to handle transient viscous flow problems. The flow structure inside the nozzle is very complex as either overexpansion or underexpansion will occur and viscous regions near the wall will become prevalent. The Euler and Navier-Stokes models are both found useful to study the starting characteristics of the nozzle flow.

The physical domain displayed in Fig. 2b is mapped onto the computational domain with the aid of a mapping function established via GRAPE. To show the versatility of mapping, the computational domain has been inverted with respect to the physical domain. Two systems of grid are used; one is

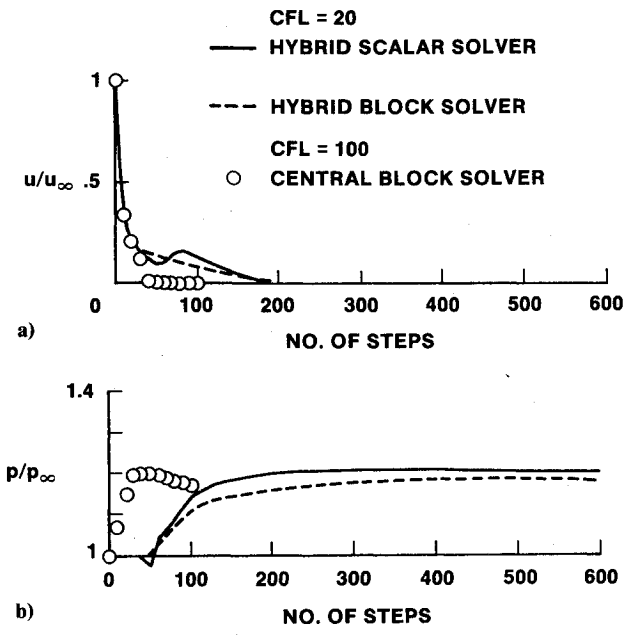

Fig. 9 Comparison of convergence history for flow variables at the inviscid shock incident location: a) velocity on the grid line next to the wall; b) pressure on the wall.

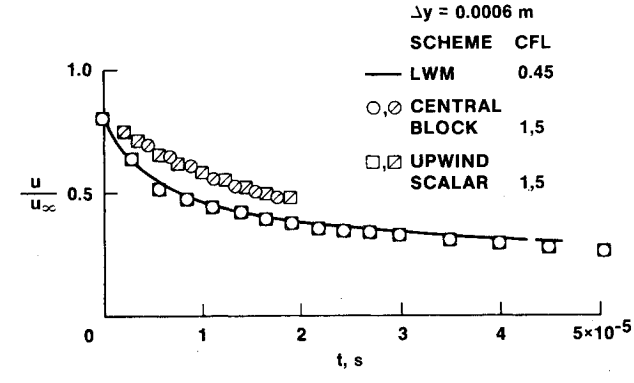

Fig. 10 Comparison of transient velocity between explicit and implicit solutions on the grid line next to the wall.

(35×15) for the inviscid model and the other is (35×28) with $\Delta y_2 = 0.003$ m next to the nozzle wall for the viscous model. The nozzle has an axial length of 4.58 m and a radius of 1.83 m at the exit. The flow features are studied in three cases: the inviscid model with slip wall, the inviscid model with no-slip wall, and the viscous model. The CFL numbers 1 and 3, respectively, for the inviscid and viscous models. Numerical experiments have indicated that the transient boundary layer varies in a time scale at least one order of magnitude lower than that of transient inviscid flow, and a CFL number greater than 3 would cause instability problems. The outflow boundary treated by the characteristics and extrapolation procedures described in earlier sections is satisfactory as long as the boundary layer remains attached to the wall. However, when the reversed flow occurs on the boundary and the flow characteristics change from hyperbolic or parabolic to elliptic, the space extrapolation is not a physically sound procedure and leads to serious errors.

A complete history of the internal viscous flow development is shown in Fig. 7 at $t = 5$, 10, 15, and 20 ms. Figures 7 and 8 are complemented to each other and help visualize the developing flowfield. The shock on the inflow boundary at $t = 0$ has moved to the midsection of the nozzle at $t = 5$ ms, and flow has begun to expand at the corner. By $t = 10$ ms, the initial shock has already moved out the nozzle, and another shock is formed because the nozzle flow overexpands. The expansion at the throat is strong and affects the entire throat area. As time increases to $t = 15$ ms, the shock due to overexpansion moves to the exit plane. No pressure gradient is seen near the wall, as the boundary layer contains a large reversed-flow bubble. At $t = 20$ ms, the axial overexpanding flow produces a stronger shock, while a vortex formed near the exit occupies one-third of the radial coordinates.

The complex nature of the transient internal flow has made this problem the most difficult one to solve. The central block method cannot handle the rapid expansion at the throat or the Mach disk formation in the midsection of the nozzle, and the MacCormack explicit method is not as efficient as the present method when the separated boundary layer has a large region of reversed flow.

Rate of Convergence and Transient Accuracy

Although the scalar method yields reasonably accurate steady results and has shown excellent shock-capturing properties, it has more restrictive stability bound than the block method. Even accounting for the difference in computation time per step, the conventional block method is still more efficient in seeking the asymptotic steady-state solution. Figure 9 shows their convergence history for the shock/boundary-layer separation problem. However, the central operator used by the block method is susceptible to instability due to large gradient of flow properties; hence, its usage is generally limited to flow with weak discontinuities.

The temporal accuracy for viscous flow solutions is evaluated on the basis of the explicit solutions. Figure 10 shows that the transient solutions of the MacCormack scheme and of the two implicit methods using CFL = 1 are nearly identical. The implicit solutions (either the block or the scalar method) have poor accuracy using CFL = 5. This simple test indicates that the error introduced by the factorization process overwhelms the errors caused by the inconsistency between explicit and implicit operators and by the approximation involved in the boundary calculations.

Conclusions

An implicit scalar method based on hybrid upwind and central schemes has been evaluated by its applications to internal and external flow problems. The shock-capturing capability is excellent, the boundary treatment is general enough to consider both inviscid and viscous inflows or outflows, and the solution is stable under severely impulsive initial and boundary conditions. The results have shown that it yields superior accuracy to and requires less computation time per integration step than the conventional central block method for viscous flowfield with strong gradients. Its transient accuracy is comparable to that of explicit methods if the Courant number is kept small. Since the predominant concern in the calculation of unsteady, viscous flowfields is an optimal balance between computation cost and solution accuracy, the present formulation and the numerical algorithm appear to have satisfied that need.

Acknowledgments

The author is grateful to the reviewer for his advice on the implicit aspects of transient solution, to Dr. Szema of Rockwell Science Center for pointing out errors in Table 1, and to Mr. Jim Duncan of Omniplan Corporation for his skillful editing of the paper.

References

[1] Li, C. P., "Simulation of Solid Rocket Startup Transient Flow Using a Numerical Method," *Proceedings of the JANNAF 13th Plume Technology Meeting*, Vol. 1, CPIA Publ. 357, April 1982, pp. 343-358.

[2]Briley, W. R. and McDonald, H., "Solution of the Multidimensional Compressible Navier-Stokes Equations by a Generalized Implicit Method," *Journal of Computational Physics*, Vol. 24, 1977, pp. 372-397.

[3]Beam, R. M. and Warming, R. F., "An Implicit Factored Scheme for the Compressible Navier-Stokes Equations," *AIAA Journal*, Vol. 16, 1978, pp. 393-402.

[4]Chaussee, D. S. and Pulliam, T. H., "Two-Dimensional Inlet Simulation Using a Diagonal Implicit Algorithm," *AIAA Journal*, Vol. 19, Feb. 1981, pp. 153-159.

[5]Moretti, G., "The λ-Scheme," *Computers and Fluids*, Vol. 7, Sept. 1979, pp. 191-205.

[6]Chakravarthy, S. R., "The Split-Coefficient Matrix Method for Hyperbolic Systems of Gas Dynamic Equations," AIAA Paper 80-0268, Jan. 1980.

[7]Steger, J. L. and Warming, R. F., "Flux Vector Splitting of the Inviscid Gas-Dynamic Equations With Application to Finite Difference Methods," *Journal of Computational Physics*, Vol. 40, 1981, pp. 263-293.

[8]Reklis, R. P. and Thomas, P. D., "A Shock Capturing Algorithm for the Navier-Stokes Equations," *AIAA Journal*, Vol. 20, Sept. 1982, pp. 1212-1218.

[9]Serra, R. A., "Determination of Internal Gas Flow by a Transient Numerical Technique," *AIAA Journal*, Vol. 10, May 1972, pp. 603-611.

[10]Yee, H. C., Beam, R. M., and Warming, R. F., "Boundary Approximations for Implicit Schemes for One-Dimensional Inviscid Equations of Gasdynamics," *AIAA Journal*, Vol. 20, Sept. 1982, pp. 1203-1211.

[11]Sorenson, R. L., "A Computer Program to Generate Two-Dimensional Grids About Airfoils and Other Shapes by the Use of Poisson's Equation," NASA TM-81198, May 1980.

[12]MacCormack, R. W., "The Effects of Viscosity in Hypervelocity Impact Cratering," AIAA Paper 69-345, May 1969.

[13]Li, C. P., "A Mixed Explicit-Implicit Splitting Method for the Compressible Navier-Stokes Equations," *Proceedings of the 5th International Conference on Numerical Methods in Fluid Dynamics, Lecture Notes in Physics*, Vol. 59, Springer-Verlag, 1976.

[14]Hakkinen, R. J., Greber, I., Trilling, L., and Abarbanel, S. S., "The Interaction of an Oblique Shock Wave with a Laminar Boundary Layer," NASA Memo 2-18-59W, 1959.

[15]Engquist, B. and Osher, S., "One-Sided Difference Approximations for Nonlinear Conservative Laws," *Mathematical Computations*, Vol. 36, April 1981, pp. 321-351.

From the AIAA Progress in Astronautics and Aeronautics Series...

SHOCK WAVES, EXPLOSIONS, AND DETONATIONS—v. 87
FLAMES, LASERS, AND REACTIVE SYSTEMS—v. 88

Edited by J. R. Bowen, University of Washington,
N. Manson, Université de Poitiers,
A. K. Oppenheim, University of California,
and R. I. Soloukhin, BSSR Academy of Sciences

In recent times, many hitherto unexplored technical problems have arisen in the development of new sources of energy, in the more economical use and design of combustion energy systems, in the avoidance of hazards connected with the use of advanced fuels, in the development of more efficient modes of air transportation, in man's more extensive flights into space, and in other areas of modern life. Close examination of these problems reveals a coupled interplay between gasdynamic processes and the energetic chemical reactions that drive them. These volumes, edited by an international team of scientists working in these fields, constitute an up-to-date view of such problems and the modes of solving them, both experimental and theoretical. Especially valuable to English-speaking readers is the fact that many of the papers in these volumes emerged from the laboratories of countries around the world, from work that is seldom brought to their attention, with the result that new concepts are often found, different from the familiar mainstreams of scientific thinking in their own countries. The editors recommend these volumes to physical scientists and engineers concerned with energy systems and their applications, approached from the standpoint of gasdynamics or combustion science.

Published in 1983, 505 pp., 6×9, illus., $39.00 Mem., $59.00 List
Published in 1983, 436 pp., 6×9, illus., $39.00 Mem., $59.00 List

TO ORDER WRITE: Publications Order Dept., AIAA, 1633 Broadway, New York, N.Y. 10019